BIBECHANA
Vol. 20, No. 1, April 2023, 92-102

ISSN 2091-0762 (Print), 2382-5340 (Online)
Journal homepage: http://nepjol.info/index.php/BIBECHANA
Publisher:Dept. of Phys., Mahendra Morang A. M. Campus (Tribhuvan University)Biratnagar

Properties of dust in the North-East part of Perseus Cloud within the open cluster IC 348 using data from IRIS and AKARI

Surakshya Bhattarai[1], Madhu Sudan Paudel[2], Shiv Narayan Yadav[3] Ajay Kumar Jha[1,*]

[1]*Central Department of Physics, Tribhuvan University, Nepal*
[2]*Department of Physics, Tri-Chandra Multiple Campus, Tribhuvan University, Nepal*
[3]*Department of Physics, Patan Multiple Campus, Tribhuvan University, Nepal*

[*]Corresponding author. Email: ajay.jha@cdp.tu.edu.np,astroajay123@gmail.com

Abstract

In this work, we have studied the dust properties of the North-East part of Perseus cloud having a size of 0.5° × 0.5° located at RA (ICRS): 56.14° DEC (ICRS): +32.15°, within the Open Cluster IC 348, using IRIS and AKARI data. An isolated region of size 0.39°×0.23° in IRIS and 0.34°×0.16° in AKARI data is detected within it. The infrared fluxes extracted using Aladin v11.0 are used to study the dust temperature and dust mass. The distance of the selected dust structure is calculated using Gaia EDR3, which is 309.98 pc. The infrared flux density is found to be increased for long-wavelength data. The average dust color temperature calculated from short-wavelength IRIS data is more than that calculated from long-wavelength AKARI data, which are 26.34 K±0.11 K for IRIS and 17.63 K±0.02 K for AKARI data. The mass of dust within the entire dust structure is 0.06 $M_\odot$ for IRIS data and 37.44 $M_\odot$ for AKARI data. Jeans mass for isolated region gives contradictory results in two surveys, for IRIS survey total mass is smaller than Jeans mass but for AKARI survey the total mass is larger than the Jeans mass. A good correlation between infrared fluxes is noticed for linear regression. The study background sources observed from the SIMBAD database explore the large number of stars, X-ray sources, YSOs, etc., embedded within the dust structure; some of them are responsible for dust heating and some for the contribution of dust mass. The contour map shows the identical distribution between infrared fluxes, dust color temperature and Planck's function and dissimilar distribution between dust mass and visual extinction in IRIS and AKARI data. The high temperature at the central region suggests that the core of dust structure is thermally active, radiating the large thermal radiation in comparison to the outer region.

Keywords
Perseus Molecular Cloud, IC 348, IRIS, AKARI, Dust Color Temperature, Dust Mass.

Article information
Manuscript received: November 22, 2022; Accepted: April 4, 2023
DOI https://doi.org/10.3126/bibechana.v20i1.49392

1 Introduction

Molecular clouds are the most important structure in the interstellar medium (ISM) as they are the birthplace of the star. Milky Way galaxy has hundreds of known molecular clouds out of which Perseus Molecular Cloud is one of the nearby Giant Molecular Cloud (GMC) which extends at distance from 293 pc to 321 pc from us [1]. It occupies the size of $6^o \times 2^o$ in the Perseus Constellation and holds 10^4 M$\odot$ gas and dust [2]. Most of the Perseus Molecular Cloud is invisible in optical wavelength, only two parts; Open Cluster IC 348 and NGC 1333 are visible in optical wavelength, but it is bright at mid and far-infrared wavelengths due to the radiation coming from dust heated by a large number of young low-mass stars [3].

Open Cluster IC 348 is located in the North-East part of Perseus Cloud which contains the old stars in comparison to the West part. There is many research about the age of the IC 348. Based on Hα emission from the stars in IC 348 Herbig(1998) [4] estimated the age between 0.7 to 12 Myr [4]. Luhman(1998) [5] declared that most of the stars in IC 348 are younger than 3 Myr but some stars has been formed 10 Myr ago [5]. In other research, Muench(2003) [6] calculated the mean age of stars $\sim$ 2 Myr with a fluctuation of $\sim$ 3 Myr [6]. The variation of the age of stars in IC 348 indicates the two episodes of star formation. The smaller value of mean age represents the majority of younger stars which might have been formed due to the dissolved core of Perseus Cloud and the old age is the indication of low-mass stars from Perseus OB2 association. Due to the dominance of young stars a , huge emission due to dust in far-infrared wavelength is observed in IC 348 cluster [6].

The infrared wavelength is the most crucial electromagnetic radiation in the sense that it can explore those regions of the galaxy which is invisible for optical and other short-wavelength radiation. The interstellar dust is the least contributing component of ISM by mass but is very important to control the heating and cooling mechanism including complex chemical processes. Interstellar dust absorbs the UV and other energetic radiation and re-radiates the absorb energy in the form of infrared radiation. In this way, infrared wavelength is the way to explore the interstellar dust within the galaxy [7].

In past, many research has been performed exploring the properties of interstellar dust using the infrared data in the region near the Pulsars [8, 9], White Dwarfs [10,11], AGB Star [12,13], Supernova Remnants [14, 15], FIR loops [16–18][, FIR Cavities [18, 19], Isolated Nebula [20], etc., using the data from IRAS, IRIS and AKARI. In this work, we have used the data from IRIS and AKARI to explore the properties of dust within the molecular cloud. The dust color temperature and dust mass of the region in the North-East part of Perseus Cloud within the IC 348 is calculated and possible physical processes are explained.

2 Materials and Methodology

2.1 Data

In this work, we have taken data from four different sources. The IRIS data [21] at 60 μm and 100 μm and AKARI data [22] at 90 μm and 140 μm are used to calculate and compare results. The FITS images in both IRIS and AKARI surveys are downloaded from SkyView Virtual Observatory (https://skyview.gsfc.nasa.gov/current/cgi/query.pl) and infrared flux density is extracted using Aladin v2.5 and v11.0 [23]. We used the Gaia EDR3 from Gaia Archive (https://gea.esac.esa.int/archive) for the estimation of the distance to the dust structure. The SIMBAD database (http://simbad.u-strasbg.fr/simbad/sim-fcoo) is used to study the background sources within the dust structure.

2.2 Method

2.2.1 Dust color temperature estimation

The calculation of dust color temperature from the IRIS 60 μm and 100 μm flux densities is done following the Wood et al. (1994) [24] and Schnee et al. (2005) [25]. The final expression for the temperature for IRIS 60 μm to 100 μm data is,

$$T_d = \frac{-0.96}{\ln(R \times 0.6^{(3+\beta)})} \quad (1)$$

where R is the ratio of the flux densities at 60 μm and 100 μm and β is the spectral emissivity index, which takes the value from 0 to 2 for different materials. In this work, we used the β=2 assuming the dust as the crystalline dielectric [26]. Following the Wood et al. (1994) [24], the equation (1) can be changed for AKARI 90 μm and 140 μm as given by;

$$T_d = \frac{-0.57}{\ln(R \times 0.64^{(3+\beta)})} \quad (2)$$

2.2.2 Dust mass and Jeans mass estimation

We have followed the calculation of Young et al. 1993 [27] and Hildebrand 1983 [28] to estimate the dust mass. The dust mass depends on the physical and chemical properties of the dust grains, the dust temperature (T_d) and the distance (D) to the

object. The expression of dust mass is;

$$M_d = 0.4\left(\frac{S_v D^2}{B(\nu, T_d)}\right) \quad (3)$$

where S_v= F(100 μm)×5.288 × 10^{29} kg s^2 for IRIS = F(140 μm)×5.288 × 10^{29} kg s^2 for AKARI, B(ν,T_d) is the Planck's function for blackbody radiation given by,

$$B(\nu, T_d) = \frac{2h\nu^2}{c^2}\left(\frac{1}{e^{\frac{h\nu}{k_B T_d}} - 1}\right) \quad (4)$$

where, the symbols have the usual meaning. The Jean's mass gives the critical mass of matter within the cloud that needed to trigger the star formation process within the Molecular Cloud. It depends on the average temperature, density and size of the cloud. Once we know the size and temperature of the region we can calculate the density using [7];

$$\rho = \left(\frac{3}{4\pi}\right)^{2/3}\left(\frac{k_B T_d}{m_H G R^2}\right) \quad (5)$$

where, k_B is the Boltzmann constant, T_d is dust color temperature, m_H is the mass of hydrogen G is the universal gravitational constant and R is the radius of the Molecular Cloud considering the spherical shape. The Jean's mass can be calculated using the formula [7];

$$M_J = \left(\frac{k_B T_d}{m_H G}\right)^{3/2}\left(\frac{1}{\rho^2}\right) \quad (6)$$

2.2.3 Visual extinction

The loss of the radiation by the process of scattering and absorption is called the extinction. Dust are the vital component for the extinction in interstellar medium. The visual extinction refers the extinction of visible light coming from the star caused by the dust. Following the Wood et al. (1994) [24], the visual extension is given by;

$$A_v = 15.078\left(1 - exp\frac{-T_\lambda}{641.3}\right) \quad (7)$$

where, $T_\lambda = F(\lambda)/B(v, T_d)$ is the optical thickness and is the infrared flux density at long wavelength (100 μm for IRIS and 140 μm for AKARI) in SI unit, and represents Planck function at long wavelength.

2.2.4 Inclination angle

The inclination angle is the angle made by the line of sight to the perpendicular of the plane of the dust structure. For the calculation of inclination angle, we use Holmberg (1946) [29] formula given by,

$$\cos^2 i = \left(\frac{\left(\frac{b}{a}\right)^2 - q^{*2}}{1 - q(*)^2}\right) \quad (8)$$

where a and b are the major to minor diameter and q* is the intrinsic flatness of the structure. The intrinsic flatness gives the information of internal morphology of the cloud. The value of intrinsic flatness is taken from 0.23 for Molecular Cloud [30].

3 Results and Discussion

3.1 Contour levels in FITS image

In this work, the FITS image of the selected dust structure around Open Cluster IC 348 in Perseus Cloud located at RA (ICRS): 56.14^o, DEC (ICRS): +32.15^o is processed in the Aladin v2.5 and v11.0 software [23]. The data of infrared flux of all 0.5^o × 0.5^o sized regions is extracted from all FITS images, 60 μm and 100 μm in IRIS and 90 μm and 140 μm in AKARI. Also, we draw isocontours based on infrared flux in long-wavelength image (100 μm in IRIS and 140 μm in AKARI) to find the isolated region. In IRIS 100 μm image, the isocontour at level 42, named Outer-42, with infrared flux 153.43±2.24 MJy sr^{-1} is the largest possible contour. The other isocontours are Middle-93 with flux 292.85±6.69 MJy sr^{-1} and Inner-171 with flux 507.29±10.29 MJy sr^{-1}. In AKARI 140 μm image the isocontour at level 80, named as Outer-80, with infrared flux 325.47±0.71 MJy sr^{-1} is the largest possible contour. The other isocontours are Middle-18 with flux 489.30±1.20 MJy sr^{-1}, Inner–167 (Up) with flux 570.90±1.93 MJy sr^{-1} and Inner–167 (Down) with flux 575.95±1.64 MJy sr^{-1}. The dust structure with the contours levels, geometrical center, position of maximum and minimum flux and temperature and major and minor axis are shown in Figure 1.

3.2 Infrared flux density

The infrared flux is the basic parameter in this work from which we have calculated the dust color temperature and dust mass. For the extraction of infrared flux, the IRIS images of size 20 pixel×20 pixel are used so that there are total 400 data. In AKARI data we use the image of size 100 pixel ×100 pixel so that there are 10,000 data. The flux density from all FITS images (60, 100, 90 and 140 μm) are extracted using Aladin v11.0 [23]. These values of infrared flux are used to calculate the dust color temperature and dust mass within the selected structure. The statistical details of infrared flux is given in

Table 1. In IRIS 60 μm and 100 μm data the maximum value of flux is found at the same position but they have a different value. Similarly, in AKARI 90 μm and 140 μm data the maximum and minimum values of flux are at the same position but with a different value. The position of extreme values of flux in IRIS and AKARI data are at the slightly different positions but they are very close to each other in all four wavelengths. The detail of maximum and minimum infrared flux at all wavelengths with their respective position is given in Table 2.

Table 1: The table gives the statistical information of infrared flux in both IRIS and AKARI data.

	IRIS		AKARI	
	F(60 μm)(MJy sr^{-1})	F(100 μm)(MJy sr^{-1})	F(90 μm)(MJy sr^{-1})	F(140 μm)(MJy sr^{-1})
Max.	460.42	642.52	792.59	859.97
Min.	7.31	31.32	23.82	86.07
Average	60.54	143.81	107.51	255.17
Range	453.11	611.22	768.76	773.89
SD	77.70	120.25	105.62	143.32
SE	3.88	6.01	1.06	1.43

Table 2: The table gives the coordinate of maximum and minimum value of infrared fluxes and temperature observed in IRIS and AKARI data.

Survey	Quantity	Maximum Value	Coordinate [RA, DEC (ICRS)]	Minimum Value	Coordinate:[RA, DEC (ICRS)]
IRIS	F(60 μm)	460.42 MJysr^{-1}	56.16^o, +32.16^o	7.31 MJy sr^{-1}	56.42^o, +31.91^o
	F(100 μm)	642.52 MJy sr^{-1}	56.16^o, +32.16^o	31.31 MJy sr^{-1}	56.42^o, +31.91^o
	T_d	34.48 K	55.23^o, +32.17^o	23.10 K	56.32^o, +32.02^o
AKARI	F(90 μm)	792.59 MJy sr^{-1}	56.15^o, +32.15^o	23.82 MJy sr^{-1}	56.45^o, +31.91^o
	F(140 μm)	859.96 MJy sr^{-1}	56.18^o, +32.15^o	86.07 MJy sr-1	56.45^o, +32.11^o
	T_d	25.94 K	56.16^o, +32.17^o	15.37 K	56.27^o, +32.01^o

Table 3: Comparison of statistics of dust color temperature in total structure and isolated region in both IRIS and AKARI data.

	IRIS		AKARI	
	$(T_d)_{Total}$ (K)	$(T_d)_{Isolated}$ (K)	$(T_d)_{Total}$ (K)	$(T_d)_{Isolated}$ (K)
	F(60μm)$MJysr^{-1}$	F(100μm)MJy sr^{-1}	F(90μm)MJy sr^{-1}	F(140)MJy sr^{-1}
Max.	34.48	34.48	25.94	25.94
Min.	23.10	24.04	15.37	15.55
Average	26.34	28.68	17.63	19.54
Range	11.37	10.44	10.57	10.38
SD	2.20	2.19	1.60	2.13
SE	0.11	0.20	0.02	0.04

3.3 Dust color temperature

The dust color temperature of each pixel is calculated using the ratio of infrared fluxes at two wavelengths as suggested by equations (1) and (2) for both IRIS and AKARI data. We choose the value of $\beta = 2$ assuming the dust in the form of crystalline dielectric [26]. The region of maximum and minimum temperature are noted in both IRIS and AKARI data, which is presented in Table 2. In IRIS data the dust color temperature varies from 34.48 K±4.07 K to 23.10 K±1.62 K with an average value of 26.34 K± 0.11 K and range 11.38 K±2.84 K. In isolated region within the Outer–40 contour, the maximum, minimum, average and range of temperature are found to be 34.48 K±2.90 K, 24.04 K±2.32 K, 28.68 K±0.20 K and 10.44 K±2.61 K respectively. In AKARI data the dust color temperature varies from 25.94 K±4.15 K to 15.37 K±.13 K with an average value of 17.63 K±0.02 K and range 10.57 K±2.64 K. In isolated region within the Outer–80 contour, the maximum, minimum, aver-

Table 4: The table presents the dust mass and gas mass within the whole structure and isolated region in IRIS and AKARI data. The last column includes the Jeans mass within the.

Survey	$(M_d)_{Total}$	$(M_g)_{Total}$	$(M_d)_{Isolated}$	$(M_g)_{Isolated}$	(M_J)
IRIS	1.11×10^{29} kg (0.06 M⊙)	2.22×10^{31} kg (11.14 M⊙)	5.00×10^{28} kg (0.03 M⊙)	1.00×10^{31} kg (5.03 M⊙)	1.49×10^{32} kg (74.90 M⊙)
AKARI	7.45×10^{31} kg (37.44 M⊙)	1.49×10^{34} kg (7488.59 M⊙)	1.86×10^{31} kg (9.34 M⊙)	3.72×10^{33} kg (1871.82 M⊙)	8.13×10^{31} kg (40.90 M⊙)

Table 5: The different parameters related to the linear relationship between the two infrared fluxes in IRIS and AKARI data.

Quantity	IRIS	AKARI
Slope	0.63	0.67
Y–intercept	- 29.49	- 64.20
r^2 coefficient	0.94	0.83
Average T_d	31.76 K	21.69 K

age and range of temperature are found to be 25.94 K±3.20 K, 15.55 K±1.99 K, 19.54 K±0.04 K and 10.38 K±2.60 K respectively. In both data, large fluctuation of temperature in the whole dust structure as well as in the isolated region suggests that the region is highly affected by the external factor.

3.4 Dust mass and Jeans mass

The dust mass is estimated by using equation (3). For the calculation of the mass, we need the distance to the dust structure. The dust structure is within Open Cluster IC 348 in the well-known Perseus cloud. We have estimated the distance to the selected dust structure using the data from Gaia EDR3, which is found to be 309.98 pc. This is very close to the distance of the Open Cluster IC 348 from literature 315 pc [5]. We calculate the mass of the structure in each pixel. The sum of the masses of all the pixels gives the total mass of the dust within the structure. After calculating the dust mass, the mass of gas is calculated by using fact that the mass of the gas in ISM is about 200 times greater than the mass of the dust [31]. Using that concept to the mass gas within the structure is calculated. For the estimation of Jeans mass, we need average size, density and average temperature. The average size of the structure is calculated by converting the angular dimension into a linear dimension using the relation, linear dimension = distance × angular dimension. It gives the major and minor diameters. The average radius of the isolated structure is 0.85 pc or 2.60×10^{16} m for the IRIS image and 0.68 pc or 2.08×10^{16} m for the AKARI image. This shows that the isolated region is smaller in the AKARI image. We use the average temperature of the isolated region 28.68 K for the IRIS data and 19.54 K for AKARI data. The density of the dust in the isolated region is calculated using equation (5), which is 2.02×10^{-18} kgm^{-3} for IRIS data and 2.14×10^{-18} kgm^{-3} in AKARI data. Using all these values in equation (6), Jeans Mass (M_J) is calculated using both IRIS and AKARI data, given in Table 4. From the table, it is seen that almost half of the total mass is contained within the isolated region. For AKARI data the total mass is higher in comparison to IRIS data, this is due to the higher resolving capacity of the AKARI data. For IRIS data the, Jeans mass is greater than the total mass of the gas but for the AKARI data, the Jeans mass is less than the total mass of gas within the isolated region. This gives the contradictory result. However, it can be interpreted that in AKARI data the size of the isolated structure is small as well the average temperature is small in comparison to the IRIS data. This might be the possible reason that the isolated in AKARI data appears a possible star-forming region whereas the isolated region in IRIS data is not the possible star-forming region.

3.5 Relation between infrared fluxes

The relation between flux density obtained from 100 μm and 60 μm in IRIS and 140 μm and 90 μm in AKARI is studied using linear regression. We plotted the flux at a long-wavelength (100 μm in IRIS and 140 μm in AKARI) towards X-axis and flux at a short-wavelength (60 μm in IRIS and 90 μm in AKARI) towards the Y-axis. Figure 2 shows the linear relation between infrared fluxes. The slope of the straight line gives the ratio of flux which can be used to estimate the average dust color temperature. Table 5 shows the various information related to the linear plot. This average temperature is quite different from the average temperature estimated in Table 3. This might be due to the large value of Y-intercept obtained in the equation. Because, our ex-

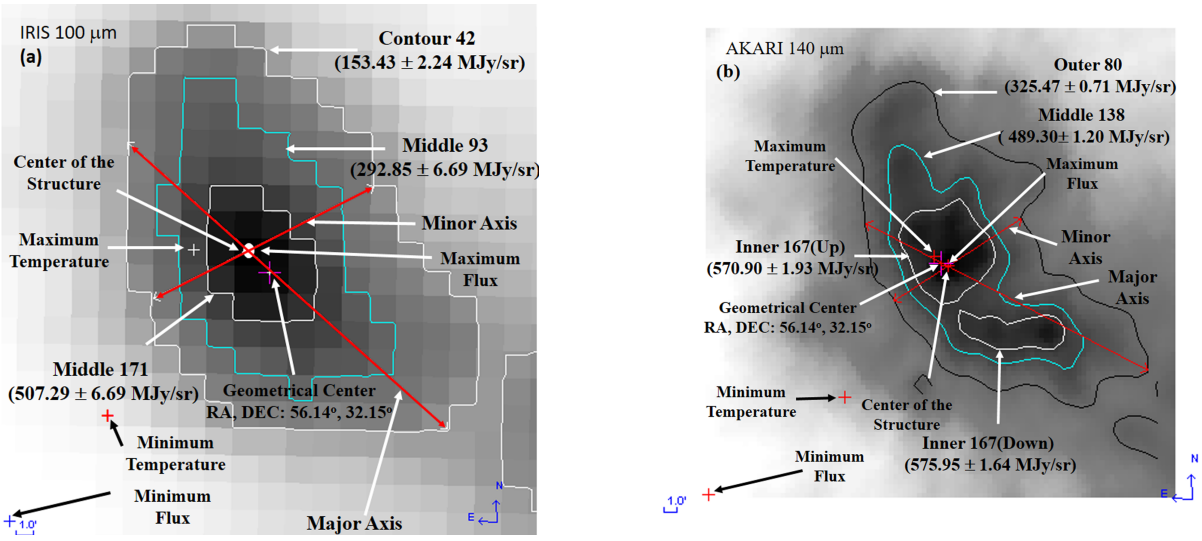

Figure 1: Figure shows the $0.5^o \times 0.5^o$ size view of FITS image in Aladin v2.5 with center at RA (ICRS): 56.14^o DEC (ICRS): + 32.15^o showing three contours along with the position of geometrical center, center of structure with maximum flux, minimum flux, maximum temperature, minimum temperature and contours levels in 100 μm IRIS image (a) and 140 μm AKARI image (b) within the Open Cluster IC 348 in the Perseus Cloud.

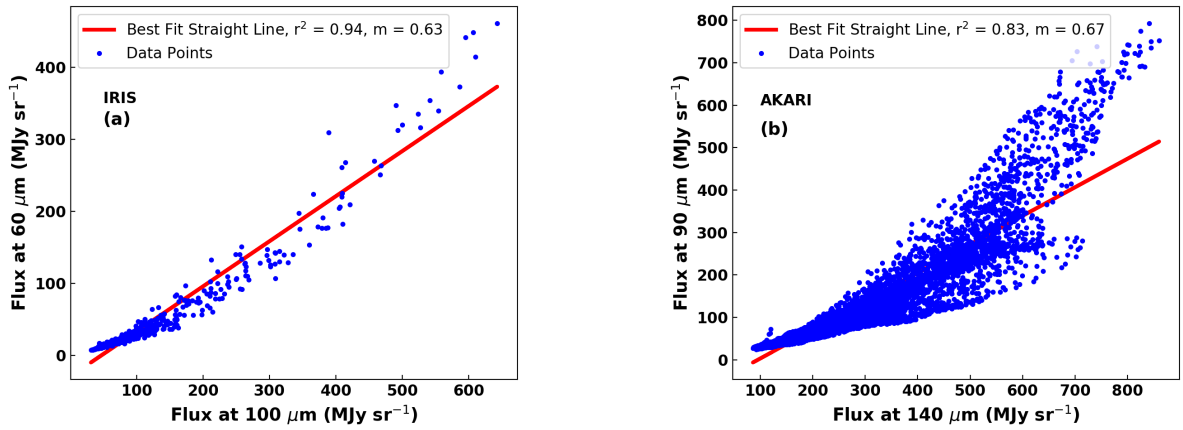

Figure 2: The graph shows the best fit linear relation between infrared flux density at two wavelengths. In graph, flux at 100 μm (IRIS) and 140 μm (AKARI) are taken along X-axis and flux at 60 μm (IRIS) and 90 μm (AKARI) are taken along Y - axis. The straight line shows the best fitted straight, r^2 and m represents the regression coefficient and slope of the straight line.

Table 6: The table presents the contour levels, major and minor diameter and inclination in both IRIS and AKARI data. There are three contours in IRIS data and four contours in AKARI data.

IRIS				AKARI			
Contours	a (arcmin)	b (arcmin)	i (deg)	Contours	a (arcmin)	b (arcmin)	i (deg)
Outer-42	23.59	13.80	56.48	Outer-80	20.30	9.67	64.65
Middle-93	18.89	9.18	63.94	Middle-138	14.93	6.69	66.76
Inner-171	8.57	4.80	58.38	Inner–167 (Up)	6.78	5.12	42.37
—-				Inner–167(Down)	6.72	2.12	77.22

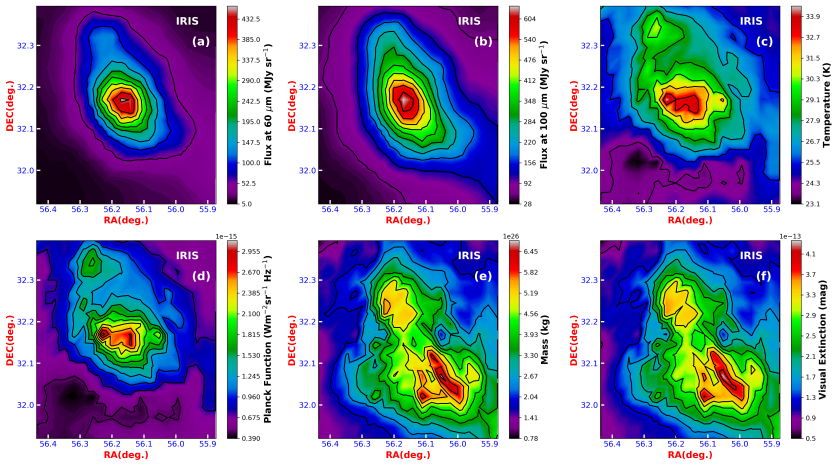

Figure 3: The figure shows the contour map for infrared flux at 60 μm (a), infrared flux at 100 μm (b), dust color temperature (c) Planck's function (d), dust mass (e), and visual extinction (f). In all figure RA taken is along X - axis, DEC is taken along Y – axis and all these quantities are represented by color bar. The lines represents the isocontours for respective quantities.

pectation was the equation in the form of y = mx, a straight line passing through the origin. However, the regression coefficient shows a very good correlation between the data.

3.6 Contour map

The variation of intensity of infrared fluxes in two wavelength, dust color temperature, Planck's function, dust mass and visual extinction is studied using a contour map as is shown in Figure 3. In the contour map, it is seen that the distribution of infrared flux density is very much similar to each other in both IRIS and AKARI data. The infrared flux density for long wavelengths (100 μm in IRIS and 140 μm in AKARI) is greater than the infrared flux density at short wavelength (60 μm in IRIS and 90 μm in AKARI). In all wavelengths the infrared flux density is high towards the central region and low towards the lower-left corner. The intensity of infrared flux decreases gradually from the center towards the outer region in all wavelengths. On the other hand, the contour map of dust temperature and Planck's function are similar to each other in both IRIS and AKARI data. This is because Planck's function is simply a function of temperature at a particular wavelength. Furthermore, it shows that the temperature, as well as the thermal radiation intensity, is maximum at the central region. This suggests that the central region is thermally active in comparison to the outer region. The lower left region is most thermally stable. The contour map of dust mass and visual extinction is similar. The distribution pattern is slightly different in IRIS and AKARI data. Which might be due to the difference in the resolution of the image. This similarity indicates that the thick dust can cause more visual extinction. The mass distribution shows that the dust is concentrated in the lower belt, especially in the lower right regions in comparison to the other regions.

3.7 Simbad background sources

The background objects around the dust structure are studied using the SIMBAD database (http://simbad.u-strasbg.fr/simbad/sim-fcoo). There are 2665 sources in the square region of size $0.5^o \times 0.5^o$ within the dust structure. The maximum number of objects are star, young stellar objects (YSO), X-ray source, T Tauri star, variable star of Orion type, sub-millimetric radio source, part of the cloud, etc. There are many other sources which are less in number but they are very important

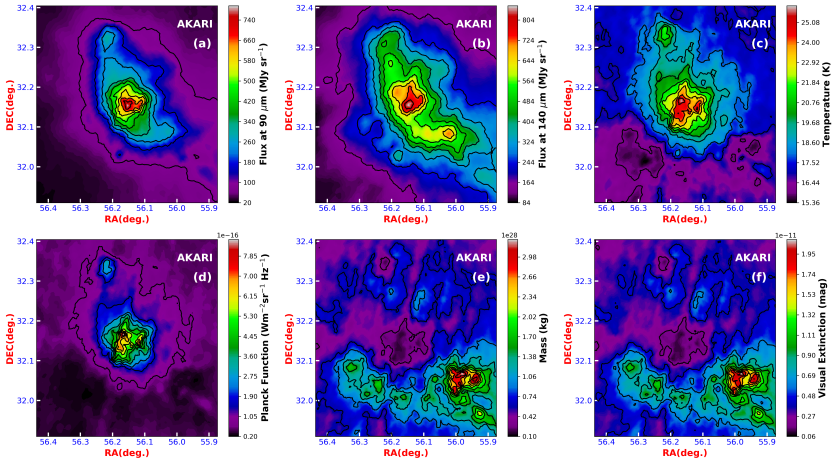

Figure 4: The figure shows the contour map for infrared flux at 90 μm (a), infrared flux at 140 μm (b), contour map for dust color temperature (c), Planck's function (d), dust mass (e) and visual extinction (f). In all figure RA taken is along X - axis, DEC is taken along Y - axis and these quantities are represented by color bar. The lines represents the isocontours for respective quantities.

for contributing the dust mass within the structure under study. The mass of the dust is higher within the lower belt of the structure and maximum in the lower right portion. In this region the ISM components, such as; part of cloud, dense core, sub-millimetric radio source, radio source, Herbig-haro object, infrared source, far–infrared sources are presented densely, as shown in Figure 5.

3.8 Gaussian Plot

The Gaussian distribution with histogram is used to study the normal behavior of the distribution of dust color temperature and dust mass within the dust structure. In Figure 6 we can see the Gaussian distribution of dust color temperature and dust mass with a histogram. It is seen that for dust color temperature the Gaussian distribution is very close to the Normal distribution. But for dust mass, the Gaussian distribution deviates from the Normal distribution. This shows that the distribution of dust color temperature is more symmetric than the dust mass. The slight deviation of the Gaussian distribution of dust mass from the Normal distribution might be due to the presence of ISM sources, such as; dense core, part of the cloud, radio (sub-mm) source, etc., present in the lower belt of the dust structure observed in the SIMBAD database.

3.9 Inclination angle

For the calculation of inclination angle, we have calculated the major and minor axis of all contours using Aladin v2.5. Figure 1 shows the Aladin v2.5 view of the FITS image with three-level contour and major and minor diameter for the outermost contour. The major and minor diameters for the other contours are not shown in Figure 1. The inclination angle is calculated using equation (8). For IRIS data, the inclination angle first increases from Outer-42 to Middle-93 and decreases from Middle-93 to Inner-171. In AKARI data, there is a similar fluctuation observed in inclination angle from outer to inner contours. Both data indicate that the isolated region is non-uniform and irregularly distributed in the morphological point of view. Also, the value of inclination angle for outer contour indicates the isolated region is edge-on in both IRIS and AKARI data because i $> 45^o$. The brief information about the major axis, minor axis and corresponding inclination angle for all contours in both IRIS and AKARI data are presented in Table. 6 below.

4 Conclusion

In this work, the infrared flux, dust color temperature and dust mass of the dust structure around Open Cluster IC 348 in Perseus Cloud, located at RA (ICRS): 56.14^o, DEC (ICRS): $+32.15^o$ is studied. Following are the major conclusions of this work;

- The size of the dust structure is $0.5^o \times 0.5^o$, which consists of an isolated dust region of size $0.39^o \times 0.23^o$ in IRIS and $0.34^o \times 0.16^o$ in AKARI data. The size of the isolated region is smaller in AKARI data.
- The average and minimum value of infrared flux density are increased from short-wavelength to long-wavelength but this trend is violated for maximum value.
- The average dust color temperature of dust

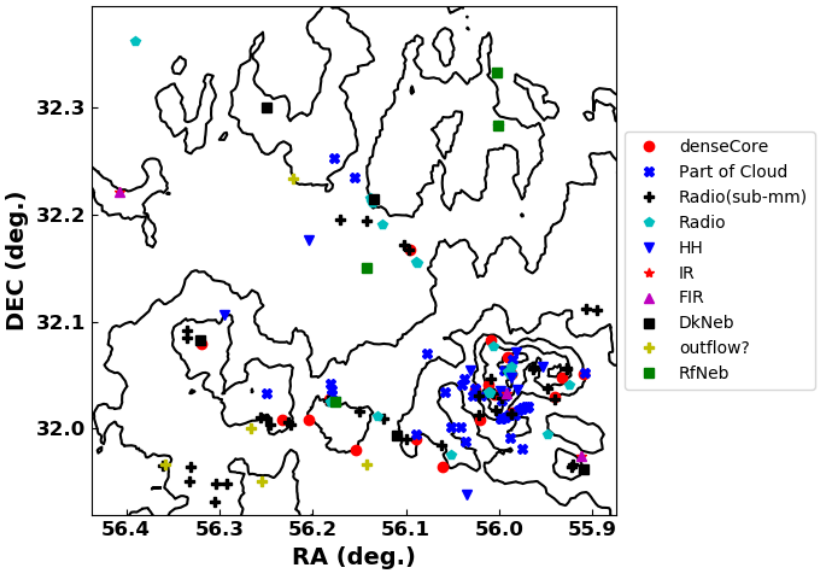

Figure 5: The objects within the background of the dust structure which might be responsible for the contribution of dust mass are shown in the figure. The contours are same as the isocontour for dust mass in AKARI data. In the figure region in which the density of these objects is more the mass of dust is found higher, especially in AKARI data.

structure is found 26.34 K±0.11 K in IRIS and 17.63 K±0.02 K for AKARI data. The low temperature in long-wavelength region is according to the Wien's displacement law.

- The study of contour map shows the distribution between infrared fluxes in all wavelengths, and temperature and Planck's function in both IRIS and AKARI data are similar. The contour map of Planck's function shows that the intensity of thermal radiation is maximum at the central region.

- The central part of the isolated region is hotter than the outer region representing the central region is thermally active and the outer region is thermally stable. The lower left region is thermally most stable.

- Contour map of dust map and visual extinction shows an identical distribution representing that the dense dust causing more extinction. However, a clear difference is observed between IRIS and AKARI data.

- The distance of the dust structure is estimated using Gaia EDR3, which is found to be 309.98 pc. This value of the distance is very close to the distance of the Open Cluster IC 348 from the literature.

- The study of background sources in the SIMBAD database explores the objects which might be responsible for the contribution of dust temperature and dust mass within the dust structure.

- The total mass of gas in isolated structure is found more in AKARI data (3.72×10^{33} kg) than in IRIS data (1.00×10^{31} kg). The Jeans mass for the isolated structure is 1.49×10^{32} kg for IRIS data and 8.13×10^{31} kg for AKARI data. This indicates that the structure formation via gravitational collapse is possible according to AKARI data only.

- The Gaussian distribution is very close to the Normal curve for dust color temperature slight deviation from the Normal curve for dust mass. This might be due to the asymmetric distribution of ISM sources, such as; dense core, part of cloud, radio (sub-mm) source, etc., which are observed in the SIMBAD database.

- The study of inclination angle shows that the isolated region within the dust structure is edge-on in both data. Also, the isolated region is non-uniform and irregularly distributed from the morphological point of view.

Acknowledgments

We acknowledge Central Department of Physics, Tribhuvan University, Nepal, Tri-Chandra Multiple Campus, Tribhuvan University, Nepal and Patan

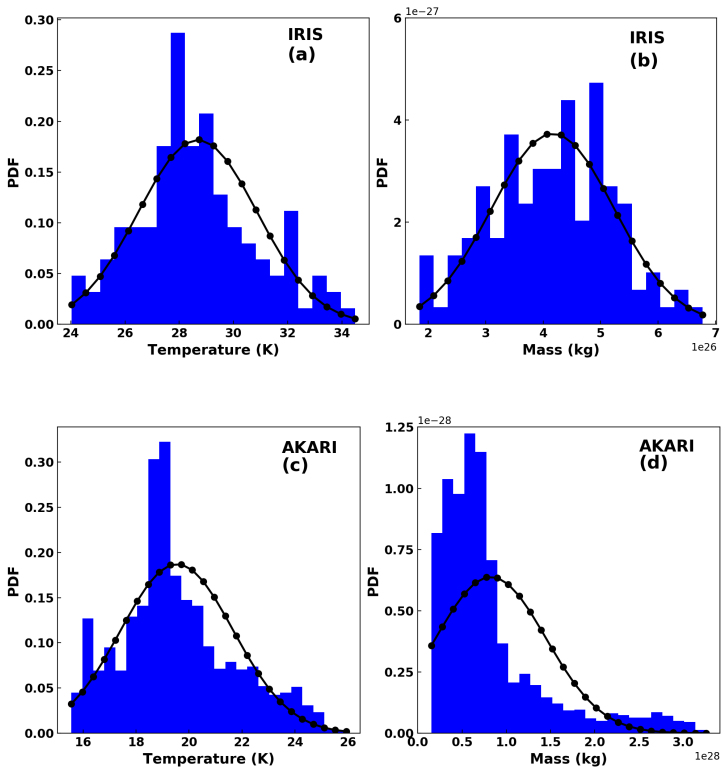

Figure 6: Gaussian distribution for dust color temperature and dust mass in isolated region of both IRIS and AKARI data.

M. Campus, Tribhuvan University, Nepal for providing the academic environment. We are also grateful to the Sky View Virtual Observatory, SIMBAD, IRIS, AKARI, and Gaia Archive for the source of data. Two authors (AKJ SNY) acknowledge UGC, Nepal for providing a faculty research grant no.FRG-075/076-ST-2. We are thankful to the anonymous referee for his/her comments.

References

[1] N Gisela and et al. The gould's belt distances survey (gobelins). v. distances and kinematics of the perseus molecular cloud. *The Astrophysical Journal*, 865(1):73, 2018. 10.3847/1538-4357/aada49

[2] H Ungerechits and P Thaddeus. A co survey of the dark nebula in perseus, taurus and auriga. *The Astrophysical Journal Supplement Series*, 63:645–660, 3 1987.

[3] J Bally, J Walawender, D Johnstone, H Kirk, A Goodman, and B Reipurth. *Handbook of Star Forming Regions 1*, volume 1. 2008.

[4] GH Herbig. The young cluster ic 348. *The Astrophysical Journal*, 497(2):736, 1998.

[5] KL Luhman, JR Stauffer, AA Muench, GH Rieke, EA Lada, J Bouvier, and CJ Lada. A census of the young cluster ic 348. *The Astrophysical Journal*, 593:1093, 2003.

[6] AA Muench, EA Lada, CJ Lada, R Elston, J Alves, M Horrobin, TL Huard, J Levine, S Raines, and CG Román-Zúñiga. A study of the luminosity and mass functions of the young ic 348 cluster using flamingos wide-field near-infrared images. *The Astronomical Journal*, 125:2029, 2003. 10.1086/373925

[7] H Karttunen, P Kröger, H Oja, M Poutanen, and KJ Donner. *Fundamental astronomy, Vol. 4*, volume 4. Springer, 2007. 10.1007/978-3-540-34144-4

[8] A. K. Jha and B. Aryal. A study of a pulsar wind driven structure in far-infrared iras map at latitude 10°. *Journal of Institute of Science and Technology*, 22(1):1–9, 2017. 10.3126/jist.v22i1.17733

[9] A. K. Jha and B. Aryal. A study of a cavity nearby a pulsar at-60º latitude in the far infrared map. *Journal of Nepal Physical Society*, 4(1):33–41, 2017. 10.3126/jnphyssoc.v4i1.17334

[10] I. N. Joshi, A. K. Jha, and B. Aryal. A study of dust structure nearby white dwarf wd1334-678. *BIBECHANA*, 18(2):130–137, 2021. 10.3126/bibechana.v18i2.37439

[11] M. S. Paudel, P. Bhandari, and S. Bhattarai. Study of dust cavity around the white dwarf wd 0352-049 in infrared astronomical satellite map. *Journal of Nepal Physical Society*, 7(2):110–118, 2021. 10.3126/jnphyssoc.v7i2.38631

[12] A. K. Jha and D. R. Upadhyay. Dust structure around two asymptotic giant stars at latitude 32° & 40.67°. *Himalayan Physics*, pages 41–47, 2017. 0.3126/hj.v6i0.18356

[13] S. P. Gautam, A. Silwal, M. Tiwari, S. Subedi, M. Khanal, and A. K. Jha. Dust properties of two new cavity structures nearby asymptotic giant branch stars: The iras survey. *Journal of Institute of Science and Technology*, 26(2):119–126, 2021. 10.3126/jist.v26i2.41556

[14] A K Jha, A Yadav, D R Upadhyay, and B Aryal. Dust properties of super-nova remnant (crab nebula) using akari survey. *Journal of Nepal Physical Society*, 7(4):64–70, 2021. doi.org/10.3126/jnphyssoc.v7i4.42933

[15] M S Paudel and S Bhattarai. Studies of the properties of dust structure nearby the supernova remnants g053.41+00.3, g053.9+00.2 and g053.1+00.3 using data from iris and akari. *Journal of Nepal Physical Society*, 7(3):59–66, 2021. 10.3126/jnphyssoc.v7i3.42192

[16] A K Jha, B Aryal, and R Weinberger. A study of dust color temperature and dust mass distributions of four far infrared loops. *Revista mexicana de astronomía y astrofísica*, 53(2):321–332, 2017.

[17] A K Jha and B Aryal. A study of far infrared loop at-5o galactic latitude around pulsar j1627-5547. *BIBECHANA*, 15:70–78, 2018. 10.3126/bibechana.v15i0.18443

[18] A K Jha and B Aryal. Dust color temperature distribution of two fir cavities at iris and akari maps. *Journal of Astrophysics and Astronomy*, 39(2):1–7, 2018. 10.1007/s12036-018-9517-6

[19] M Tiwari, SP Gautam, A Silwal, S Subedi, A Paudel, and A K Jha. Study of dust properties of two far infrared cavities nearby asymptotic giant branch stars under infrared astronomical satellite maps. *Himalayan Physics*, pages 60–71, 2020. 10.3126/hp.v9i01.40193

[20] A. S. Thapa, M. S. Paudel, and B. Pant. An infrared survey of isolated nebular structures at galactic latitudes 16.98o 1.98o in aras map. *Journal of Nepal Physical Society*, 5(1):74–84, 2019. 10.3126/jnphyssoc.v5i1.26934

[21] M. A. Miville-Deschênes and G. Lagache. Iris: a new generation of iras maps. *The Astrophysical Journal Supplement Series*, 157(2):302–305, 2005.

[22] Y. Doi, S. Takita, T. Ootsubo, K. Arimatsu, M. Tanaka, Y. Kitamura, and E. F. Cypriano. The akari far-infrared all-sky survey maps. *Publications of the Astronomical Society of Japan*, 67(3):50, 2015. 10.1093/pasj/psv022

[23] F. Bonnarel, P. Fernique, O. Bienaymé, D. Egret, F. Genova, M. Louys, F. Ochsenbein, M. Wenger, and J. G. Bartlett. The ALADIN interactive sky atlas–a reference tool for identification of astronomical sources. *Astronomy and Astrophysics Supplement Series*, 143(1):33–40, 2000.

[24] D. O. Wood, P. C. Myers, and D. A. Daugherty. Iras images of nearby dark clouds. *The Astrophysical Journal Supplement Series*, 95:457–501, 1994.

[25] S. L. Schnee, N. A. Ridge, A. A. Goodman, and J. G. Li. A complete look at the use of iras emission maps to estimate extinction and dust temperature. *The Astrophysical Journal*, 634:442–450, 2005.

[26] X. Dupace and et al. Inverse temperature dependence of the dust submillimeter spectral index. *Astronomy & Astrophysics*, 404:L11–L14, 2003. 10.1051/0004-6361:20030575

[27] K. Young, T. G. Phillips, and G. R. Knapp. Circumstellar shells resolved in iras survey data ii-analysis. *The Astrophysical Journal*, 409(2):725–738, 1993.

[28] R. H. Hildebrand. The determination of cloud masses and dust characteristics from submillimetre thermal emission. *Quarterly Journal of the Royal Astronomical Society*, 24:267, 1983.

[29] E. Holmberg. On the apparent diameters and the orientation in space of extragalactic nebulae. *Meddelanden fran Lunds Astronomiska Observatorium Serie II*, 117:3–82, 1946.

[30] M. P. Haynes and R. Giovanelli. Neutral hydrogen in isolated galaxies. iv-results for the arecibo sample. *The Astronomical Journal*, 89:758–800, 1994.

[31] T. Henning and H. Mutschke. Low-temperature infrared properties of cosmic dust analogues. *Astronomy and Astrophysics*, 327:743–754, 1997.